REGULAR ARTICLE

blood advances

Bone marrow sinusoidal endothelial cells are a site of *Fgf23* upregulation in a mouse model of iron deficiency anemia

Xiuqi Li,[1] Larisa Lozovatsky,[1] Steven M. Tommasini,[2] Jackie Fretz,[2,*] and Karin E. Finberg[1,*]

[1]Department of Pathology and [2]Department of Orthopaedics & Rehabilitation, Yale School of Medicine, New Haven, CT

Key Points

- Iron-deficient *Tmprss6*$^{-/-}$ mice show elevated circulating FGF23 levels.
- BM-SECs upregulate *Fgf23* in chronic iron deficiency anemia, in phlebotomy-induced anemia, and in response to erythropoietin treatment.

Iron deficiency is a potent stimulator of fibroblast growth factor 23 (FGF23), a hormonal regulator of phosphate and vitamin D metabolism, that is classically thought to be produced by bone-embedded osteocytes. Here, we show that iron-deficient *transmembrane serine protease 6* knockout (*Tmprss6*$^{-/-}$) mice exhibit elevated circulating FGF23 and *Fgf23* messenger RNA (mRNA) upregulation in the bone marrow (BM) but not the cortical bone. To clarify sites of *Fgf23* promoter activity in *Tmprss6*$^{-/-}$ mice, we introduced a heterozygous *enhanced green fluorescent protein* (*eGFP*) reporter allele at the endogenous *Fgf23* locus. Heterozygous *Fgf23* disruption did not alter the severity of systemic iron deficiency or anemia in the *Tmprss6*$^{-/-}$ mice. *Tmprss6*$^{-/-}$ *Fgf23*$^{+/eGFP}$ mice showed green fluorescence in the vascular regions of BM sections and showed a subset of BM endothelial cells that were GFP^{bright} by flow cytometry. Mining of transcriptomic data sets from mice with normal iron balance revealed higher *Fgf23* mRNA in BM sinusoidal endothelial cells (BM-SECs) than that in other BM endothelial cell populations. Anti-GFP immunohistochemistry of fixed BM sections from *Tmprss6*$^{-/-}$ *Fgf23*$^{+/eGFP}$ mice revealed GFP expression in BM-SECs, which was more intense than in nonanemic controls. In addition, in mice with intact *Tmprss6* alleles, *Fgf23-eGFP* reporter expression increased in BM-SECs following large-volume phlebotomy and also following erythropoietin treatment both ex vivo and in vivo. Collectively, our results identified BM-SECs as a novel site for *Fgf23* upregulation in both acute and chronic anemia. Given the elevated serum erythropoietin in both anemic models, our findings raise the possibility that erythropoietin may act directly on BM-SECs to promote FGF23 production during anemia.

Introduction

The endocrine hormone fibroblast growth factor 23 (FGF23) plays a key role in skeletal health by inhibiting renal phosphate reabsorption and suppressing circulating levels of 1,25-dihydroxyvitamin D_3 and parathyroid hormone.[1] Cells of the bone cortex (ie, osteoblasts and osteocytes) have been viewed as major sites of FGF23 expression and upregulation in physiological and pathological states.[2-4] FGF23 is secreted into the circulation both as a full-length bioactive hormone and peptide fragments generated from intracellular cleavage.[5] Circulating forms can be measured using enzyme-linked immunosorbent assays (ELISAs) that detect either intact FGF23 (iFGF23) alone or both intact hormone and C-terminal cleaved fragments, with the latter assay (cFGF23) providing insight into the total amount of FGF23 produced.[5]

Submitted 12 December 2022; accepted 5 July 2023; prepublished online on *Blood Advances* First Edition 7 July 2023. https://doi.org/10.1182/bloodadvances.2022009524.

*J.F. and K.E.F. contributed equally to this study.

Presented in abstract form at the 59th annual meeting of the American Society of Hematology, Atlanta, GA, 9 December 2017, and the 63rd annual meeting of the American Society of Hematology, Atlanta, GA, 13 December 2021.

Data are available on request from the corresponding author, Karin E. Finberg (karin.finberg@yale.edu).

The full-text version of this article contains a data supplement.

The levels of FGF23 messenger RNA (mRNA) and the circulating hormone are influenced by multiple factors, including the serum levels of phosphate,[6-8] 1,25-dihydroxyvitamin D_3,[3,8,9] parathyroid hormone,[10-12] and inflammatory cytokines.[13-18] FGF23 levels increase in patients with chronic kidney disease, where they are associated with an increased risk of cardiovascular events and mortality.[19] Initial links between iron deficiency and FGF23 regulation were observed during the study of the clinical variability of autosomal dominant hypophosphatemic rickets (ADHR), a disorder of plasma FGF23 elevation caused by defective FGF23 proteolytic cleavage[20,21]; intriguingly, serum iron is negatively correlated with circulating FGF23 levels in this disorder.[22] In the general population, serum cFGF23 shows inverse correlations with serum iron in healthy premenopausal women[23] and with serum ferritin in middle-aged men and women.[24] In older individuals, low serum iron is associated with high iFGF23[25,26] and cFGF23[26] independently from markers of inflammation[25,26] or renal impairment.[25] Furthermore, in a rural Kenyan population, with a high prevalence of iron deficiency, antenatal oral iron supplementation lowers maternal plasma cFGF23 at delivery compared with placebo.[27]

Iron deficiency also increases FGF23 levels in experimental mouse models. Both, in an ADHR model and in wild-type mice, induction of iron deficiency anemia (IDA) through dietary manipulation after weaning led to elevations in *Fgf23* mRNA from homogenized femur/tibia and in serum cFGF23.[28] In both ADHR and wild-type mice, induction of maternal iron deficiency yielded pups with elevations in femur/tibia *Fgf23* mRNA, serum cFGF23, and serum iFGF23 levels as well as hypophosphatemia at weaning age.[29] Furthermore, in wild-type mice, both inflammation-induced iron restriction and functional iron deficiency without superimposed inflammation (achieved via exogenous hepcidin administration) elevated both whole femur *Fgf23* mRNA and serum cFGF23 levels.[16]

To clarify the cellular sites of FGF23 upregulation during IDA, we used mice with genetic loss of *transmembrane serine protease 6* (*Tmprss6*), a model of the autosomal recessive disorder Iron-Refractory Iron Deficiency Anemia.[30] Because TMPRSS6, which is expressed predominantly in the liver,[31,32] dampens the hepatic production of hepcidin,[32,33] *Tmprss6* mutants exhibit chronic IDA on a standard rodent diet because of impaired absorption of dietary iron.[32] Hepcidin elevation in *Tmprss6*-knockout (*Tmprss6*$^{-/-}$) mice begins prenatally, causing anemia by the early postnatal period.[34] Notably, *Tmprss6*$^{-/-}$ mice show hepcidin elevation without markers of inflammation,[35] and their IDA phenotype does not require local *Tmprss6* expression in hematopoietic cells.[36] Here, we showed that *Tmprss6*$^{-/-}$ mice exhibit elevated circulating FGF23, and using an endogenous locus enhanced green fluorescent protein (eGFP) reporter, we established sites of *Fgf23* production (1) in chronic, genetically induced IDA, (2) in acute phlebotomy-induced anemia, and (3) after direct administration of erythropoietin (EPO).

Methods

Animal strains

Animal studies were approved by the Yale University Institutional Animal Care and Use Committee. *Tmprss6*-deficient mice (B6.129P2-*Tmprss6*^{tm1Dgen}/Crl),[33] obtained from Deltagen, and *Fgf23*^{eGFP} mice (B6.129S-*Fgf23*^{tm1Sliu}/Mmjax),[37] obtained from MMRRC-JAX, were bred and housed in the Yale Animal Resource Center with free access to food (Envigo Teklad 2018S rodent diet: 200 mg/kg iron, 1.0% calcium, and 0.7% phosphorus) and water. Breeding, genotyping, and EPO treatments are described in the supplemental Methods. Retro-orbital phlebotomy (500 μL) with saline volume replacement was performed under isoflurane anesthesia, as previously described.[38] Sex- and age-matched mice were compared, as indicated.

Blood and tissue analysis

Terminal retro-orbital blood samples were collected under ketamine/xylazine anesthesia for blood counts and serum/plasma preparation (supplemental Methods). Serum was analyzed using an iron colorimetric assay (BioVision), mouse Erythopoietin/EPO Quantikine ELISA (R&D Systems), and hepcidin-murine compete ELISA (Intrinsic LifeSciences). Plasma was analyzed using mouse/rat FGF-23 (Intact) and FGF23 (C-Term) ELISAs (Quidel). Spot urine, collected immediately before dissection, was analyzed using a Creatinine Parameter assay (R&D Systems). Serum and urine phosphate were analyzed using Phosphorus Liqui-UV (Stanbio). After euthanization, organ nonheme iron concentrations were determined via bathophenanthroline quantification.[39]

Analysis of bone and BM RNA

Mouse femurs were flushed of bone marrow with RNAse-free phosphate-buffered saline. To eliminate residual BM cells, femurs were then flushed with RNAse-free water to promote cell lysis, and the marrow cavity was scraped with endodontic files before snap freezing. Total RNA from minced, flash-frozen bone was isolated using the miRNeasy Mini Kit with on-column DNase digestion (Qiagen). BM RNA was collected via RNeasy Mini Kit with on-column DNase digestion (Qiagen) in a prior study.[40] RNA (0.5 μg) was reverse transcribed (Bio-Rad iScript cDNA Synthesis Kit) and amplified using an ABI7500 real-time polymerase chain reaction system per the supplemental Methods.

Confocal imaging

Green fluorescence in briefly fixed BM plugs was assessed via immediate imaging, using a Zeiss LSM 880 Airyscan confocal microscope. Colocalization of green fluorescence and endomucin immunofluorescence in fixed, decalcified femur cryosections was assessed using a Leica SP8 Gated STED 3× superresolution microscope (supplemental Methods).

Flow cytometry

BM endothelial cells were analyzed per the method described by Xu et al[41] (see supplemental Methods for the detailed procedure). Cell fluorescence was captured on a BD LSR II flow cytometer (Yale Flow Cytometry Facility) and analyzed using FlowJo 10.5.2.

Immunohistochemistry

Whole femurs were fixed in 10% formalin at room temperature for 3 days. Formic acid decalcification, paraffin-embedding, 5 μm sectioning, and anti-GFP immunohistochemistry were performed by Yale Pathology Tissue Services (supplemental Methods). Brightfield images were acquired using an Olympus BX40 microscope with an attached Spot Insight 4.0 Mp color digital camera.

Statistical analyses

One-way or two-way analysis of variance with Tukey post hoc test and linear regression analyses were conducted using Prism 9. $P < .05$ was considered statistically significant. Analyses and visualization of RNA-sequencing (RNA-Seq) data were performed using R (version 4.1.1) in RStudio (version 1.4.1717).

Results

Iron-deficient *Tmprss6*$^{-/-}$ mice exhibit elevated FGF23

To characterize the effects of chronic IDA on phosphate-related parameters, we generated *Tmprss6* wild-type (*Tmprss6*$^{+/+}$), heterozygous (*Tmprss6*$^{+/-}$), and knockout (*Tmprss6*$^{-/-}$) offspring with C57BL/6N genetic background that underwent phenotypic characterization at 8 weeks. Consistent with their known hepcidin elevation,[33] *Tmprss6*$^{-/-}$ mice showed hypoferremia, microcytic anemia, elevated serum EPO, and markedly reduced nonheme iron concentrations in the liver, heart, and kidney (Figure 1A-H) compared with sex-matched littermate controls. *Tmprss6*$^{-/-}$ mice also showed a greater spleen-to-body weight ratio (Figure 1I), consistent with extramedullary hematopoiesis,[33] and greater total spleen nonheme iron content (Figure 1J), consistent with macrophage iron retention.[42]

Compared with *Tmprss6*$^{+/+}$ controls, *Tmprss6*$^{-/-}$ mice exhibited a marked (600%) increase in plasma cFGF23 (Figure 1K) and a moderate (50%) increase in iFGF23 (Figure 1L). *Tmprss6*$^{+/-}$ mice showed mildly reduced liver nonheme iron concentration and signs of slight iron-restricted erythropoiesis (Figure 1F,C) but retained plasma cFGF23 and iFGF23 levels comparable with those of *Tmprss6*$^{+/+}$ controls (Figure 1K-L). *Tmprss6*$^{-/-}$ mice showed evidence of increased urinary phosphate excretion but appeared capable of compensating for the maintenance of normal serum phosphate (Figure 1M-O). Unexpectedly, *Fgf23* mRNA levels in the bone cortex did not differ significantly between the *Tmprss6*$^{-/-}$ mice and littermate controls (Figure 1P). Younger *Tmprss6*$^{-/-}$ mice also showed microcytic anemia and elevated circulating FGF23 (supplemental Figure 1). Collectively, these findings validate *Tmprss6*$^{-/-}$ mice as a model of chronic IDA with systemic FGF23 elevation.

Heterozygous *Fgf23* disruption does not alter the severity of iron deficiency in *Tmprss6*$^{-/-}$ mice

To facilitate the identification of FGF23 production sites in *Tmprss6*$^{-/-}$ mice, we introduced an established *Fgf23* reporter allele[37] in which the *eGFP* coding sequence is knocked in immediately after the endogenous *Fgf23* start codon (*Fgf23*^{eGFP}). This allele abolishes the transcription of endogenous *Fgf23* mRNA and simultaneously enables the use of eGFP to mark cells in which the *Fgf23* promoter is active. Because the *Tmprss6* and *Fgf23*^{eGFP} mouse strains differed in genetic background, we used a controlled, multigenerational breeding scheme to produce experimental *Tmprss6*$^{+/+}$, *Tmprss6*$^{+/-}$, and *Tmprss6*$^{-/-}$ littermates (F2 generation) that were either heterozygous for the *Fgf23*^{eGFP} allele (*Fgf23*$^{+/eGFP}$) or lacked the reporter (*Fgf23*$^{+/+}$) (supplemental Figure 2A). *Fgf23*$^{eGFP/eGFP}$ homozygotes, which are, in effect, *Fgf23* null, were not generated because this genotype exhibits marked growth retardation and significant mortality before weaning.[37]

Firstly, we examined whether the heterozygous loss of *Fgf23* altered hematopoietic or iron status within any *Tmprss6* genotype. Within each *Tmprss6* genotype, heterozygous *Fgf23* disruption did not significantly alter survival to weaning age (supplemental Figure 2A), adult body weight (supplemental Figure 2B-C), serum hepcidin, serum iron, hemoglobin (Hgb), red cell indices, tissue nonheme iron concentrations, spleen-to-body weight ratio, or total spleen iron content (male, Figure 2A-J; female, supplemental Figure 3A-J). Notably, the heterozygous loss of *Fgf23* did not alter the degree of hypoferremia, anemia, tissue iron deficiency, or splenomegaly in the *Tmprss6*$^{-/-}$ mice.

Compared with *Tmprss6*$^{+/+}$*Fgf23*$^{+/+}$ males, *Tmprss6*$^{-/-}$*Fgf23*$^{+/+}$ males showed significantly higher serum EPO and plasma cFGF23 and a trend toward higher plasma iFGF23 ($P = .202$; Figure 3A-C). Serum EPO, plasma cFGF23, and plasma iFGF23 in *Tmprss6*$^{-/-}$*Fgf23*$^{+/+}$ females were all significantly higher than those in the *Tmprss6*$^{+/+}$*Fgf23*$^{+/+}$ females (Figure 3D-F). In *Tmprss6*$^{-/-}$ females, the elevations in cFGF23 and iFGF23 were blunted by heterozygous *Fgf23* disruption, suggesting an *Fgf23* gene dosage effect. In other *Tmprss6* genotypes, heterozygous *Fgf23* disruption caused modest, nonsignificant reductions in mean cFGF23 levels (supplemental Figure 4A-B; note the log scales on y-axes). In *Tmprss6*$^{-/-}$*Fgf23*$^{+/eGFP}$ mice, the cFGF23 level remained significantly higher than that in nonanemic genotypes (Figure 3B,D), suggesting that this genotype would be informative for interrogating sites of increased *Fgf23* expression in the setting of IDA.

Because the mechanism leading to FGF23 upregulation in IDA is not yet known, we examined the relationship between plasma cFGF23/iFGF23 and circulating physiological parameters that are altered in IDA. When considering all mice from this cohort with 2 intact *Fgf23* alleles, serum iron and Hgb both showed significant inverse correlations with cFGF23 and iFGF23 (supplemental Figure 4C-F), whereas serum EPO showed a significant positive correlation with cFGF23 and iFGF23 (Figure 3G-H). Under a linear regression model, the correlations of cFGF23 and iFGF23 with serum EPO showed a better goodness of fit (ie, higher R^2 values) than their respective correlations with other circulating parameters (ie, serum iron and Hgb). Interestingly, EPO elevation in *Tmprss6*$^{-/-}$ females was blunted by the heterozygous *Fgf23* disruption (Figure 3D). Collectively, these findings suggested that the regulation of FGF23 and EPO may be coupled.

Tmprss6$^{-/-}$ mice show increased *Fgf23* expression in the BM

As our study was in progress, Rabadi et al[43] reported that in C57BL/6 mice, acute blood loss elevates *Fgf23* in total BM RNA. Therefore, we analyzed the *Fgf23* mRNA expression in the total BM of *Tmprss6*$^{+/+}$, *Tmprss6*$^{+/-}$, and *Tmprss6*$^{-/-}$ littermates with 2 intact *Fgf23* alleles. *Tmprss6*$^{-/-}$ mice showed significantly higher BM *Fgf23* mRNA than *Tmprss6*$^{+/+}$ controls (Figure 4A), suggesting that increased FGF23 production by 1 or more BM cell types may contribute to the elevated circulating FGF23 levels in *Tmprss6*$^{-/-}$ mice.

Next, we compared green fluorescence in briefly fixed BM core biopsies from *Tmprss6*$^{-/-}$ mice with or without the *Fgf23*^{eGFP} allele. Using confocal microscopy, green fluorescence confirmed the reporter gene expression in a subset of cells distributed

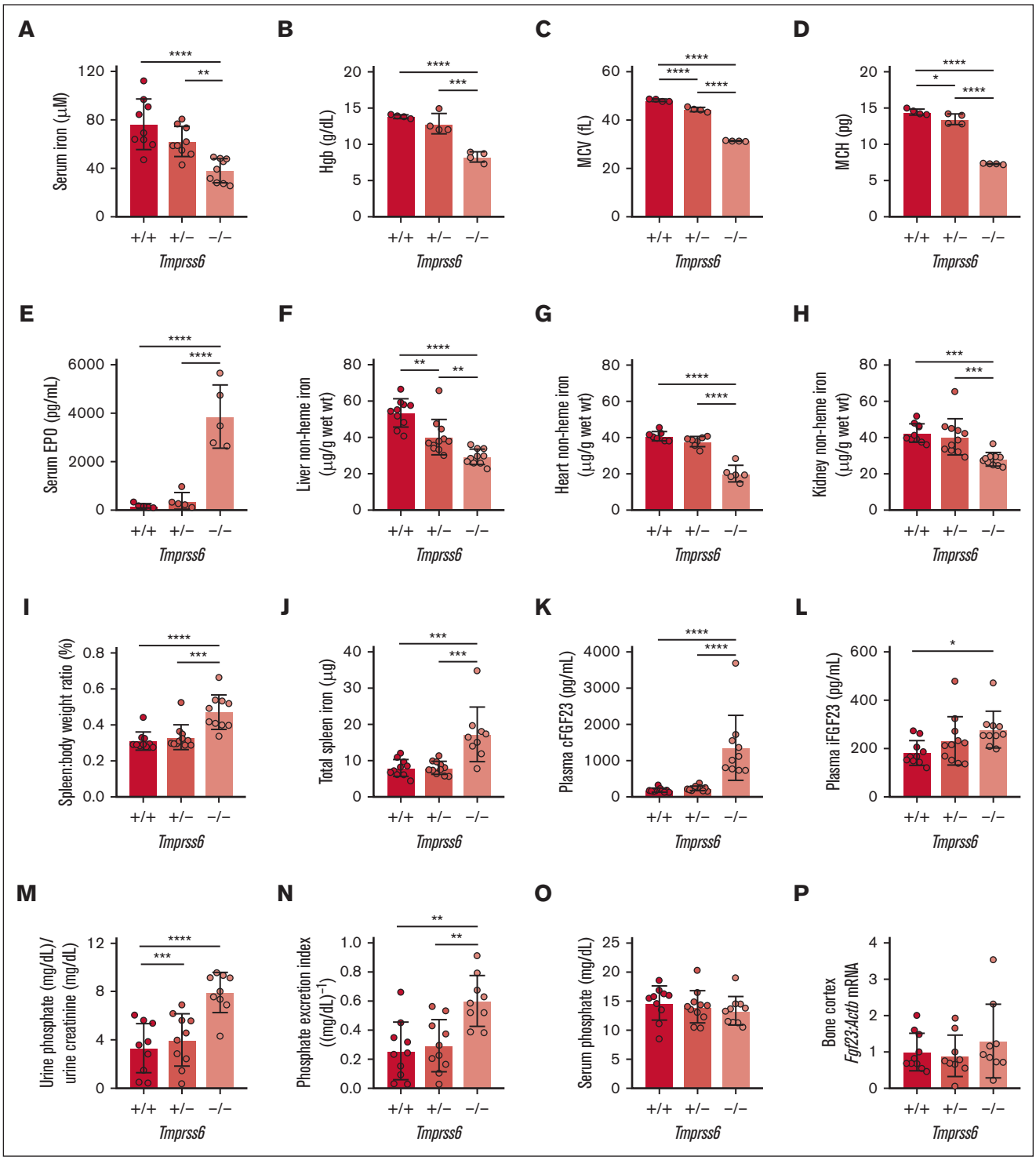

Figure 1. The perturbed iron homeostasis of *Tmprss6*$^{-/-}$ mice is accompanied by elevated FGF23 levels in circulation but unchanged *Fgf23* mRNA levels in the cortical bone. Shown for 8-week-old *Tmprss6*$^{+/+}$, *Tmprss6*$^{+/-}$, and *Tmprss6*$^{-/-}$ male littermates are (A) serum iron, (B) Hgb, (C) erythrocyte mean corpuscular volume (MCV), (D) erythrocyte mean corpuscular hemoglobin (MCH), (E) serum EPO, (F) liver nonheme iron concentration, (G) heart nonheme iron concentration, (H) kidney nonheme iron concentration, (I) spleen-to-body-weight ratio, (J) total spleen nonheme iron content, (K) plasma C-terminal FGF23 (cFGF23), (L) plasma iFGF23, (M) urine phosphate-to-creatinine ratio, (N) phosphate excretion index, (O) serum phosphate, and (P) *Fgf23* mRNA expression relative to *Actb* in the bone cortex. The mean mRNA ratio of the *Tmprss6*$^{+/+}$ mice was normalized to 1. n = 4 to 11 per group. For all graphs, data represent mean ± standard deviation. The total spleen nonheme iron content was calculated by multiplying the measured nonheme iron concentration by the total spleen weight. The phosphate excretion index was calculated as (urine phosphate ÷ serum phosphate) ÷ urine creatinine.[82] *$P < .05$; **$P < .01$; ***$P < .001$; and ****$P < .0001$ using one-way analysis of variance (ANOVA) with Tukey post hoc test.

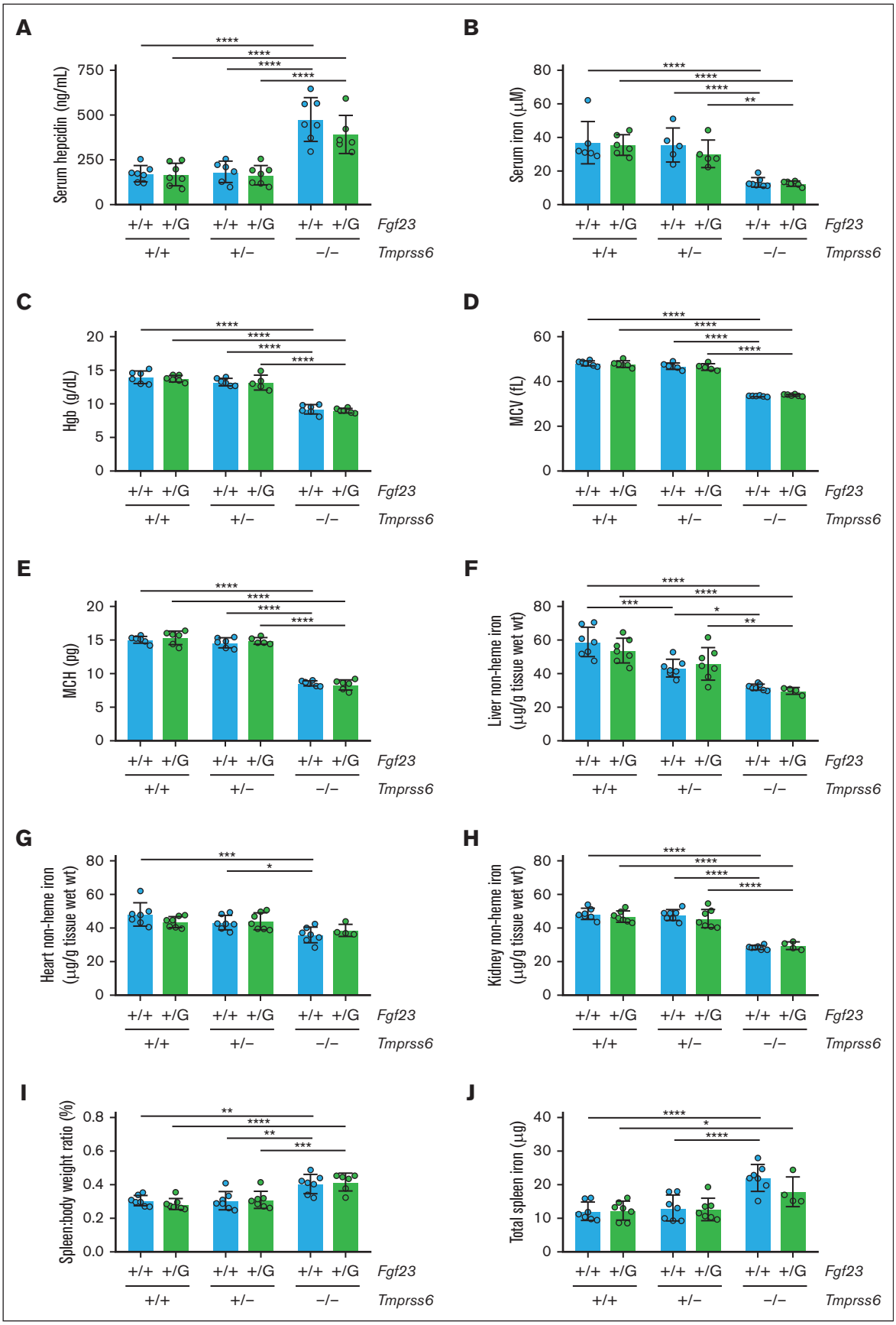
A
Serum hepcidin (ng/mL)
750
500
250
0
B
Serum iron (μM)
80
60
40
20
0
C
Hgb (g/dL)
20
15
10
5
0
D
MCV (fL)
60
40
20
0
E
MCH (pg)
20
15
10
5
0
F
Liver non-heme iron (μg/g tissue wet wt)
80
60
40
20
0
G
Heart non-heme iron (μg/g tissue wet wt)
80
60
40
20
0
H
Kidney non-heme iron (μg/g tissue wet wt)
80
60
40
20
0
I
Spleen:body weight ratio (%)
0.8
0.6
0.4
0.2
0.0
J
Total spleen iron (μg)
40
30
20
10
0
****
***
**
*
+/+ +/G +/+ +/G +/+ +/G Fgf23
+/+ +/− −/− Tmprss6

Figure 2.

throughout the BM. The elongated shape and distribution of these cells suggested their localization to the vasculature (Figure 4B). Moreover, in fixed, decalcified femur cryosections from *Tmprss6*$^{-/-}$*Fgf23*$^{+/eGFP}$ mice, fluorescence from eGFP (a cytosolic protein) in the BM showed partial overlap with the endothelial cell marker endomucin (a membrane-bound glycoprotein),[44] whereas eGFP fluorescence was absent from most osteocytes in the bone cortex and trabeculae as well as the cell populations lining the bone surfaces (Figure 4C).

To determine whether BM endothelial cells could be a site of *Fgf23* upregulation in *Tmprss6*$^{-/-}$ mice, we performed flow cytometry on BM cells harvested using an enzymatic digestion protocol that promotes the recovery of endothelial cells.[41] Bright green fluorescence was detected in a very small fraction (<0.02%) of total BM cells from mice carrying the *Fgf23*^{eGFP} allele (Figure 5). However, within the endothelial population (defined as CD45$^-$TER-119$^-$CD31$^+$),[41] cells showing bright green fluorescence were enriched (Figure 5), a finding that was confirmed using a different CD31 antibody clone (supplemental Figure 5). With both CD31 clones, the percentage of GFP^{bright} endothelial cells was higher in *Tmprss6*$^{-/-}$*Fgf23*$^{+/eGFP}$ mice than that in nonanemic mice carrying the *Fgf23*^{eGFP} reporter allele.

Sinusoidal endothelial cells show higher *Fgf23* expression than other BM stromal cell populations in mice with a normal iron balance

To clarify the BM endothelial cell subtype that expresses *Fgf23*, we interrogated published single-cell RNA-Seq (scRNA-Seq) data from the BM stromal cells of C57BL/6 mice (ie, healthy mice with no defects in iron or phosphate balance); these data were generated in a study that used unbiased clustering to define 17 stromal cell subsets, including BM sinusoidal endothelial cells (BM-SECs), arterial endothelial cells, arteriolar endothelial cells, and 2 osteolineage populations.[45] BM-SECs were the only prominent source of *Fgf23* transcripts detected in single-cell analysis (Figure 6A-B). Cells expressing *Fgf23* also expressed endothelial cell markers, such as *Pecam1* (*CD31*) and *Emcn* (*endomucin*), whereas cells expressing osteolineage markers rarely expressed *Fgf23* (Figure 6C). Several genes that lead to FGF23 dysregulation when mutated (eg, *Dmp1*,[46] *Phex*,[37] *Enpp1*,[47] and *Galnt3*[48]) were expressed in osteolineage cells but showed very low, if any, expression in BM-SECs, suggesting that FGF23 regulatory mechanisms might differ across cell types. Interestingly, mRNA encoding the *erythropoietin receptor* (*Epor*) was detected in BM-SECs. *Tmprss6* mRNA was not detected in any of the BM stromal cell populations (Figure 6C; data not shown).

By mining a different study involving bulk RNA-Seq of 4 principal stromal cell populations from wild-type murine BM,[49] we identified higher *Fgf23* expression in BM-SECs than that in BM arterial endothelial cells in mice of 3 different ages (supplemental Figure 6). Furthermore, *Fgf23* transcripts were undetectable in 2 mixed mesenchymal cell populations associated with marrow vasculature (CXCL12-abundant reticular cells and PDGFRα$^+$Sca1$^+$ cells). Collectively, our data mining suggests that BM-SECs may produce FGF23 in mice with normal iron and phosphate balance.

BM-SECs are a site of *Fgf23* upregulation in *Tmprss6*$^{-/-}$*Fgf23*$^{+/eGFP}$ mice

To assess *Fgf23*^{eGFP} reporter allele expression in the context of BM architecture, we used immunohistochemistry with an anti-GFP antibody in formalin-fixed, paraffin-embedded tissue sections, an approach that provides greater sensitivity for GFP detection than the direct visualization of fluorescence in unfixed tissue sections.[50] *Tmprss6*$^{-/-}$*Fgf23*$^{+/eGFP}$ mice showed GFP expression in BM-SECs throughout the BM, which was more intense than that in nonanemic *Tmprss6*$^{+/-}$*Fgf23*$^{+/eGFP}$ mice, and which was absent in mice lacking the *Fgf23*^{eGFP} allele (Figure 7A; supplemental Figure 7). These data identified BM-SECs as a site of *Fgf23* upregulation in mice with chronic IDA.

BM-SECs are a site of *Fgf23* upregulation in acute phlebotomy-induced anemia and after EPO injection

Because IDA in *Tmprss6*$^{-/-}$ mice results from pathologic hepcidin elevation, we also sought to determine whether BM-SECs are a site of *Fgf23* upregulation in anemic mice with intact hepcidin regulation (ie, with 2 intact *Tmprss6* alleles). We subjected *Fgf23*$^{+/eGFP}$ mice and *Fgf23*$^{+/+}$ controls to an established 500 µL phlebotomy protocol[51] (with saline volume replacement) known to induce marked anemia, EPO elevation, and hepcidin suppression. Pilot studies confirmed marked anemia and elevations of serum EPO and plasma cFGF23 in *Fgf23*$^{+/+}$ mice at 18 hours after phlebotomy (Figure 7B-E). The trajectories of hematologic recovery and EPO elevation after phlebotomy were not markedly altered by the heterozygous *Fgf23* disruption; however, phlebotomized *Fgf23*$^{+/eGFP}$ mice showed blunted plasma FGF23 responses, suggesting an *Fgf23* gene dosage effect (Figure 7E; supplemental Figure 8). Therefore, we used anti-GFP immunohistochemistry to localize the BM expression of the *Fgf23*^{eGFP} allele at baseline and 18 hours after phlebotomy. Phlebotomized *Fgf23*$^{+/eGFP}$ mice showed GFP expression in BM-SECs throughout the BM, which was more intense than that in nonphlebotomized *Fgf23*$^{+/eGFP}$ mice and absent in phlebotomized *Fgf23*$^{+/+}$ controls (Figure 7F).

Because serum erythropoietin elevation is a feature shared by *Tmprss6*$^{-/-}$ mice and mice with phlebotomy-induced anemia, we asked whether direct administration of EPO could induce *Fgf23* upregulation in BM-SECs of nonanemic mice. In BM plugs isolated from *Fgf23*^{eGFP} mice, the GFP intensity of BM-SECs was significantly higher after 18 hours of ex vivo treatment with EPO than after treatment with vehicle (supplemental Figure 9A). In addition, we assessed *Fgf23*$^{+/eGFP}$ and *Fgf23*$^{+/+}$ mice for *Fgf23*

Figure 2. Heterozygous *Fgf23* disruption does not alter iron homeostasis in mice with 2, 1, or 0 wild-type *Tmprss6* alleles. Shown for 8-week-old male mice of different *Tmprss6-Fgf23* genotype combinations are (A) serum hepcidin, (B) serum iron, (C) Hgb, (D) MCV, (E) MCH, (F) liver nonheme iron concentration, (G) heart nonheme iron concentration, (H) kidney nonheme iron concentration, (I) spleen-to-body-weight ratio, and (J) total spleen nonheme iron content. n = 4 to 7 per group. Two-way ANOVA revealed significant effects of the *Tmprss6* genotype on all parameters ($P < .001$), whereas no significant effect of the *Fgf23* genotype on any parameter was detected. For all bar graphs, data represent the mean ± standard deviation. *$P < .05$; **$P < .01$; ***$P < .001$; and ****$P < .0001$ using two-way ANOVA with Tukey post hoc test. G, *eGFP* allele.

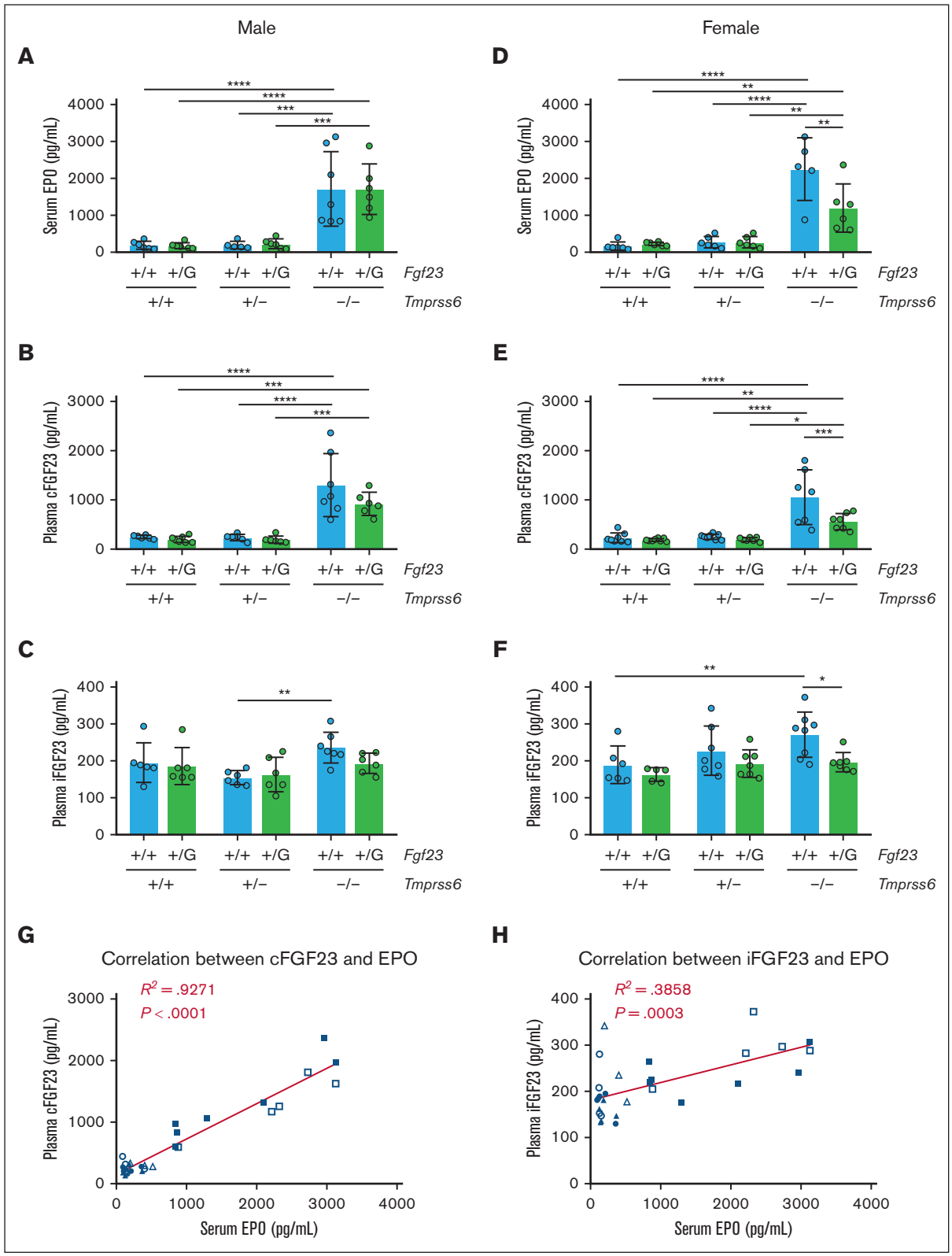

Figure 3. *Tmprss6*$^{-/-}$ mice, regardless of their *Fgf23* genotype, show EPO elevation and increased circulating levels of cFGF23. (A) Serum EPO, (B) plasma cFGF23, and (C) plasma iFGF23 of 8-week-old male mice with different *Tmprss6-Fgf23* genotype combinations (n = 5-7 per group). Using two-way ANOVA in male mice, *Tmprss6* genotype had statistically significant effects on serum EPO ($P < .0001$), plasma cFGF23 ($P < .0001$), and plasma iFGF23 ($P = .0081$), whereas the *Fgf23* genotype had no significant effect on these parameters. (D) Serum EPO, (E) plasma cFGF23, and (F) plasma iFGF23 of 8-week-old female mice with different *Tmprss6-Fgf23* genotype

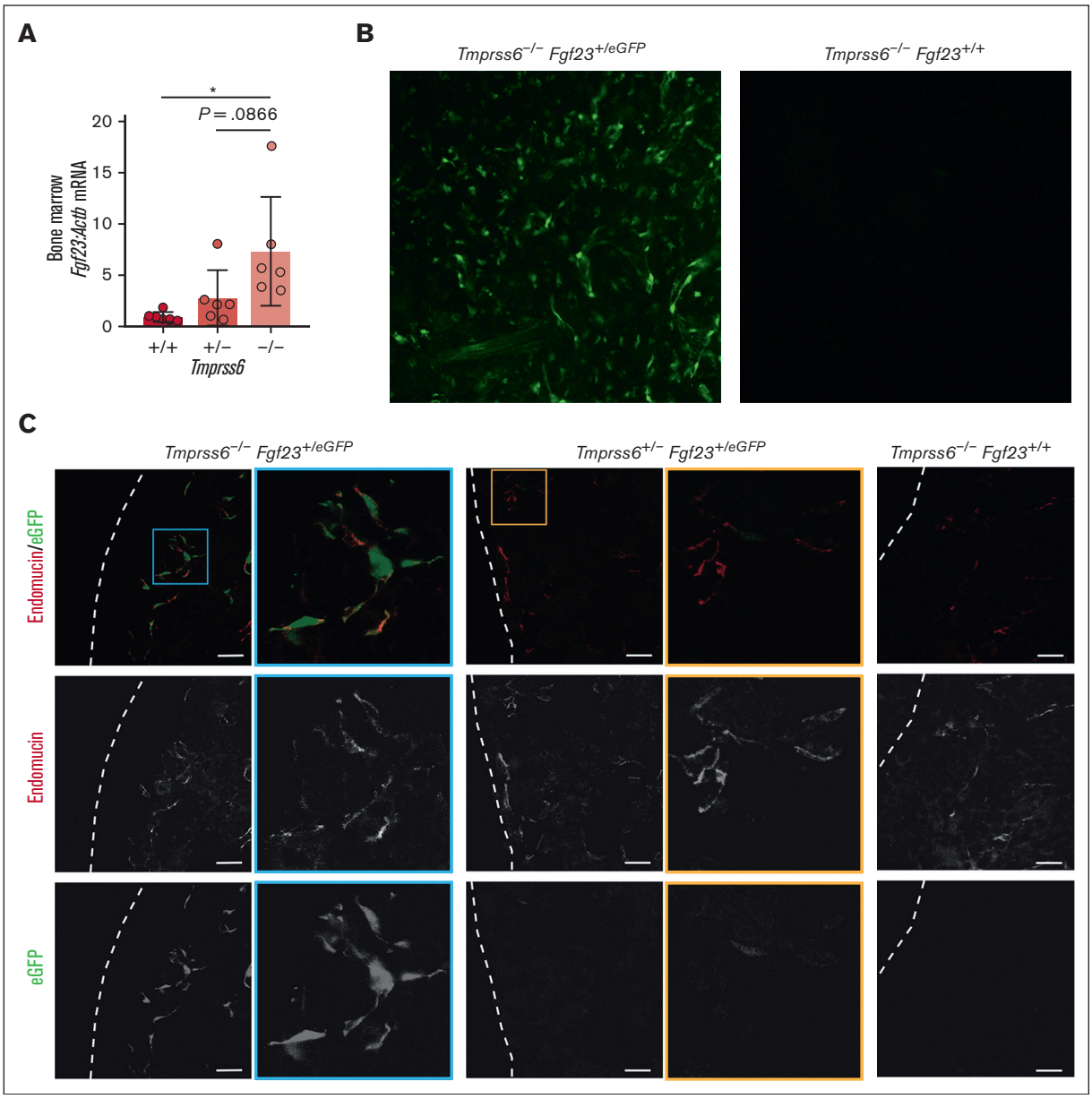

Figure 4. *Tmprss6*$^{-/-}$ mice show increased *Fgf23* expression in the BM. (A) *Fgf23* mRNA expression relative to *Actb* in the total BM mRNA of *Tmprss6*$^{+/+}$, *Tmprss6*$^{+/-}$, and *Tmprss6*$^{-/-}$ male mice (8-9 weeks old, C57BL/6 genetic background). The mean mRNA ratio of the *Tmprss6*$^{+/+}$ mice was normalized to 1. n = 7 per group; 1 outlier per genotype was identified using the Robust regression followed by OUTlier identification (ROUT) method (Q = 1%) and removed from subsequent analysis. Data represent the mean ± standard deviation. *$P < .05$ using one-way ANOVA with Tukey post hoc test. (B) Confirmation that the *Fgf23*^{eGFP} reporter allele yields green fluorescence in *Tmprss6*$^{-/-}$ BM. Shown are confocal images of briefly fixed BM core biopsies from *Tmprss6*$^{-/-}$*Fgf23*$^{+/eGFP}$ and *Tmprss6*$^{-/-}$*Fgf23*$^{+/+}$ mice (19 weeks old). Original magnification ×20. (C) Localization of green fluorescence and endomucin expression in the BM of mice carrying the *Fgf23*^{eGFP} reporter allele. Whole femurs from 6-month-male mice were fixed, decalcified, embedded, and cryosectioned before antiendomucin immunostaining. Pseudocolored merged images (GFP and endomucin) as well as individual channels in grayscale (GFP or endomucin) are presented in the same column; scale bar, 20 µm. Regions boxed in blue (*Tmprss6*$^{-/-}$*Fgf23*$^{+/eGFP}$) and yellow (*Tmprss6*$^{+/-}$*Fgf23*$^{+/eGFP}$) are presented at higher magnification in the adjacent column. The dashed line indicates the border between the bone (left) and BM (right).

Figure 3 (continued) combinations (n = 5-8 per group). Two-way ANOVA in female mice revealed statistically significant effects of both *Tmprss6* and *Fgf23* genotypes on serum EPO (*Tmprss6* genotype: $P < .0001$; *Fgf23* genotype: $P = .0297$), plasma cFGF23 (*Tmprss6* genotype: $P < .0001$; *Fgf23* genotype: $P = .0075$), and plasma iFGF23 (*Tmprss6* genotype: $P = .0191$; *Fgf23* genotype: $P = .0063$). For panels A-F, data represent mean ± standard deviation. *$P < .05$; **$P < .01$; ***$P < .001$; and ****$P < .0001$ using two-way ANOVA with Tukey post hoc test. (G) Plasma cFGF23 vs serum EPO and (H) plasma iFGF23 vs serum EPO in individual *Fgf23*$^{+/+}$ mice with different *Tmprss6* genotypes (8-week-old mice, both sexes pooled): $^{+/+}$ male (●), $^{+/-}$ male (▲), $^{-/-}$ male (■), $^{+/+}$ female (○), $^{+/-}$ female (△), and $^{-/-}$ female (□). R^2 represents the coefficient of determination using a linear regression model (ie, goodness of fit). The *P* value of the Pearson correlation is shown.

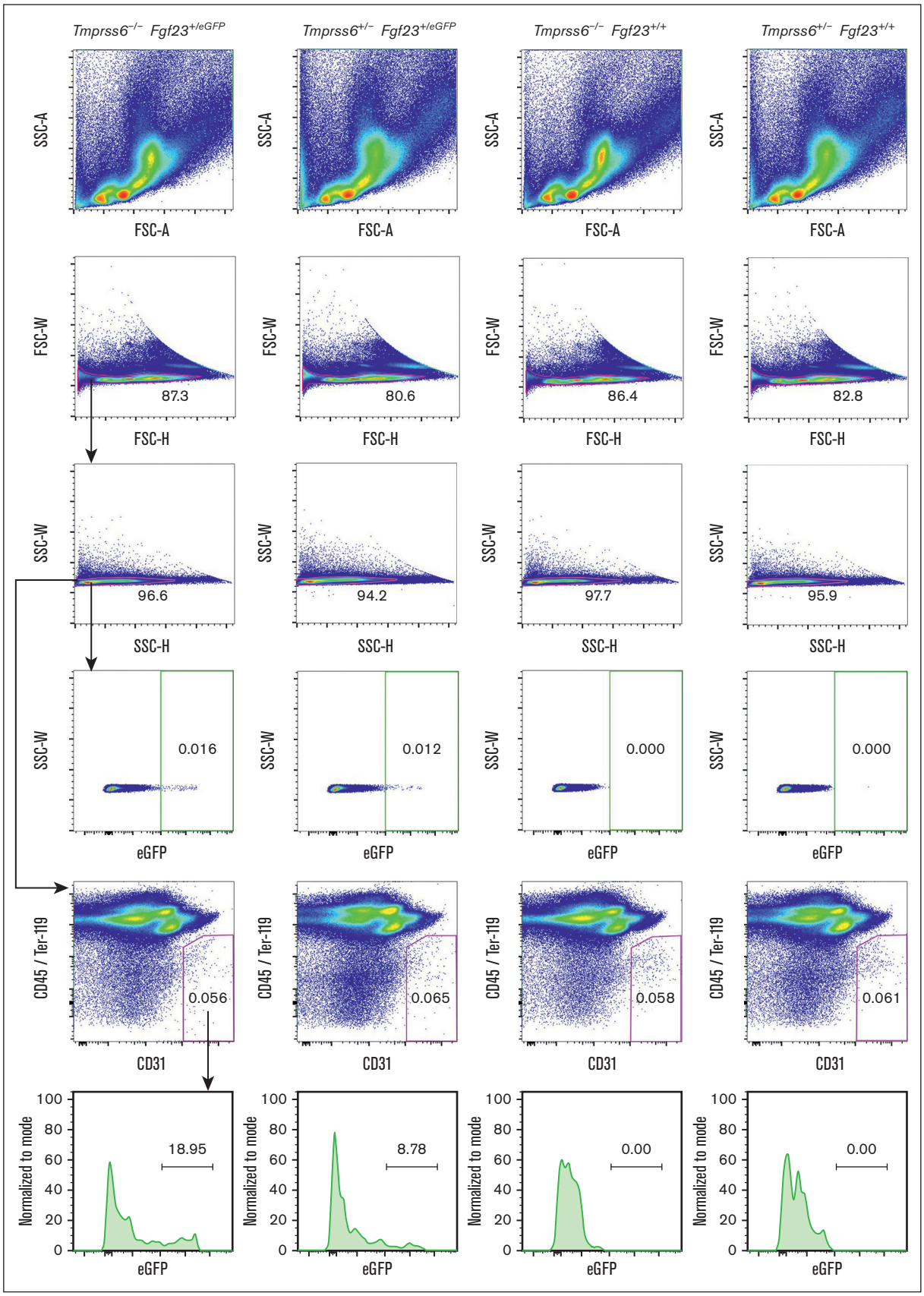
Tmprss6−/− Fgf23+/eGFP
Tmprss6+/− Fgf23+/eGFP
Tmprss6−/− Fgf23+/+
Tmprss6+/− Fgf23+/+
SSC-A
FSC-A
FSC-W
FSC-H
87.3
80.6
86.4
82.8
SSC-W
SSC-H
96.6
94.2
97.7
95.9
eGFP
0.016
0.012
0.000
0.000
CD45 / Ter-119
CD31
0.056
0.065
0.058
0.061
Normalized to mode
18.95
8.78
0.00
0.00

Figure 5.

upregulation 6 hours after injection with recombinant human EPO or saline vehicle. EPO injection significantly increased plasma cFGF23 levels (supplemental Figure 9B), consistent with results of a previous study.[52] *Fgf23*$^{+/eGFP}$ mice treated with EPO showed GFP expression in BM-SECs throughout the BM, which was more intense than that in *Fgf23*$^{+/eGFP}$ mice treated with saline and absent in EPO-treated *Fgf23*$^{+/+}$ controls (Figure 7G).

Discussion

Although iron deficiency has been associated with increased levels of circulating FGF23 in humans and mouse models, the cell type(s) contributing to the increase in FGF23 production in IDA remain unclear. Traditionally, cells of the bone cortex have been viewed as major sites of FGF23 production.[2-4] Indeed, conditional deletion of *Fgf23* in murine osteoblasts/osteocytes revealed that *Fgf23* expression in these cells maintains basal circulating FGF23 levels[53] and contributes to FGF23 elevation in response to challenges such as high-phosphate feeding[53] and induction of kidney disease.[54] However, selective deletion of *Fgf23* in osteoblasts and osteocytes reduced circulating levels of the active FGF23 hormone by only 40% or 50%,[53] suggesting that other cell types contribute to FGF23 in circulation under baseline conditions. In this study, using the *Fgf23*^{eGFP} reporter allele, we identified BM-SECs as a site of *Fgf23* upregulation in chronic genetically induced IDA and acute phlebotomy-induced anemia.

The *Fgf23*^{eGFP} reporter allele in this study was previously used by Liu et al[37] to verify osteocytes as a site of *Fgf23* upregulation in mice with pathological FGF23 elevation[55] and hypophosphatemia[56] due to the mutation of *Phex*[57] (*Phex*^{Hyp} allele). In *Phex*^{Hyp} mutants carrying the *Fgf23*^{eGFP} allele, green fluorescence was observed in the femur cortex and BM (colocalizing with CD31) as well as the thymus and brain.[37] In *Fgf23*$^{+/eGFP}$ mice with intact *Phex,* however, green fluorescence was apparent in the BM but not in the mineralized bone.[37] Compared with *Fgf23*$^{+/eGFP}$ mice with intact *Phex*, *Fgf23*$^{+/eGFP}$*Phex*^{Hyp} mice showed marked upregulation of green fluorescence in bone-embedded osteocytes but not in the BM.[37] A subsequent study found that pathological FGF23 upregulation in *Phex*^{Hyp} mice was eliminated by the selective deletion of *Fgf23* in osteoblasts/osteocytes.[53]

In our study, iron-deficient *Tmprss6*$^{-/-}$ mice showed increased circulating FGF23 compared with nonanemic controls (Figure 1K-L), which could not be attributed to higher *Fgf23* expression in osteocytes (Figure 1P). Rather, compared with nonanemic controls, *Tmprss6*$^{-/-}$ mice showed increased *Fgf23* RNA in the BM (Figure 4A) and greater *Fgf23*^{eGFP} reporter expression in BM endothelial cells (Figures 5 and 7A; supplemental Figure 5). We also observed *Fgf23*^{eGFP} reporter allele expression in rare cells of the thymus (supplemental Figure 10) but not in the liver, spleen, heart, muscle, or kidney (data not shown). Similarly, *Fgf23*$^{+/eGFP}$ mice (with intact *Tmprss6* alleles) with phlebotomy-induced anemia and elevated circulating FGF23 showed upregulation of *Fgf23*^{eGFP} reporter expression in BM-SECs compared with nonanemic *Fgf23*$^{+/eGFP}$ controls (Figure 7E).

Several groups have demonstrated that circulating FGF23 levels rise under conditions of increased erythropoietic drive. Wild-type C57BL/6 mice showed an acute increase in plasma cFGF23 (but not iFGF23) 6 hours after phlebotomy.[43] In healthy rodents, injection of recombinant human erythropoietin (rhEPO) caused significant increases in circulating cFGF23 levels[43,52,58-61] with less pronounced[52,58-61] or nonsignificant[43] changes in iFGF23 levels. Administration of rhEPO increased circulating cFGF23 levels in healthy human subjects[60] and elevated both cFGF23 and iFGF23 levels in patients with anemia of unclear etiology and normal renal function.[59] In RNA harvested from the total murine BM, upregulation of *Fgf23* mRNA was detected in response to both rhEPO injection[52,59,60] and phlebotomy,[43] and pretreatment with the BM-ablative agent carboplatin blunted the induction of circulating cFGF23 by rhEPO.[59] Different experimental approaches have suggested that erythroid,[43,60] myeloid,[60] and Lin$^-$Sca1$^+$c-Kit$^+$ cells[59] are sites of FGF23 upregulation by EPO.

In contrast, in our study, iron-deficient *Tmprss6*$^{-/-}$ mice, which also displayed EPO elevation, showed upregulated *Fgf23* reporter expression in endothelial cells in the context of intact BM architecture as well as via flow cytometry. In addition, we detected *Fgf23* mRNA in the BM-SECs of wild-type mice using scRNA-Seq[45] and bulk RNA-Seq[49] transcriptomic data sets. Our BM flow cytometric analyses used methods to enhance endothelial cell recovery (ie, enzymatic digestion and 100 μM filtering), with gating to exclude cell doublets. Notably, in our preliminary analyses conducted without enzymatic digestion, GFP^{bright} cells were not detected in the BM of the mice carrying the *Fgf23*^{eGFP} reporter allele (data not shown).

An essential role for FGF23 in phosphate and vitamin D metabolism was demonstrated in mice with a global loss of *Fgf23* (*Fgf23*$^{-/-}$), which showed hyperphosphatemia, hypervitaminosis D, reduced bone mineral content, and profound growth retardation.[62] These mice also developed other metabolic abnormalities (hypoglycemia, hypotriglyceridemia, and hypercholesterolemia), lymphoid organ atrophy, and a markedly reduced lifespan.[62] Additionally, altered frequencies of BM cell populations and aberrant red blood cell indices have been described in *Fgf23*$^{-/-}$ mouse models.[63,64] However, these hematopoietic alterations were not observed in lethally irradiated wild-type mice after transplantation with *Fgf23*$^{-/-}$ BM nucleated cells (ie, *Fgf23*$^{-/-}$ BM chimeras), suggesting that the loss of *Fgf23*$^{-/-}$ in hematopoietic cells is insufficient to alter steady-state hematopoiesis.[64] These findings in *Fgf23*$^{-/-}$ BM chimeras do not exclude the possibility that BM-SEC-derived FGF23 contributes to steady-state hematopoiesis because BM-SECs are predominantly host-derived when vascular homeostasis is restored after BM transplantation.[65,66]

Recently, a local role of FGF23 in the BM was elucidated by Ishii et al,[64] who demonstrated that FGF23 promotes the mobilization of

Figure 5. A subset of BM endothelial cells exhibit bright green fluorescence in mice that carry the *Fgf23*^{eGFP} allele. Fluorescence-activated cell sorter plots of BM cells from *Tmprss6*$^{-/-}$*Fgf23*$^{+/eGFP}$, *Tmprss6*$^{+/-}$*Fgf23*$^{+/eGFP}$, *Tmprss6*$^{-/-}$*Fgf23*$^{+/+}$, and *Tmprss6*$^{+/-}$*Fgf23*$^{+/+}$ male littermates (18 weeks old). The numbers represent the percentage of each gated population. Forward scatter (FSC) and side scatter (SSC) were used to exclude debris and cell doublets, and eGFP^{bright} cells were assessed in each single-cell population (green gate). BM endothelial cells were identified as the CD45$^-$TER-119$^-$CD31$^+$ population (magenta gate) as described,[41] using CD31 antibody clone 390, and eGFP fluorescence was assessed in the endothelial cell gate. A total of 6 × 10^5 BM cells per mouse were analyzed.

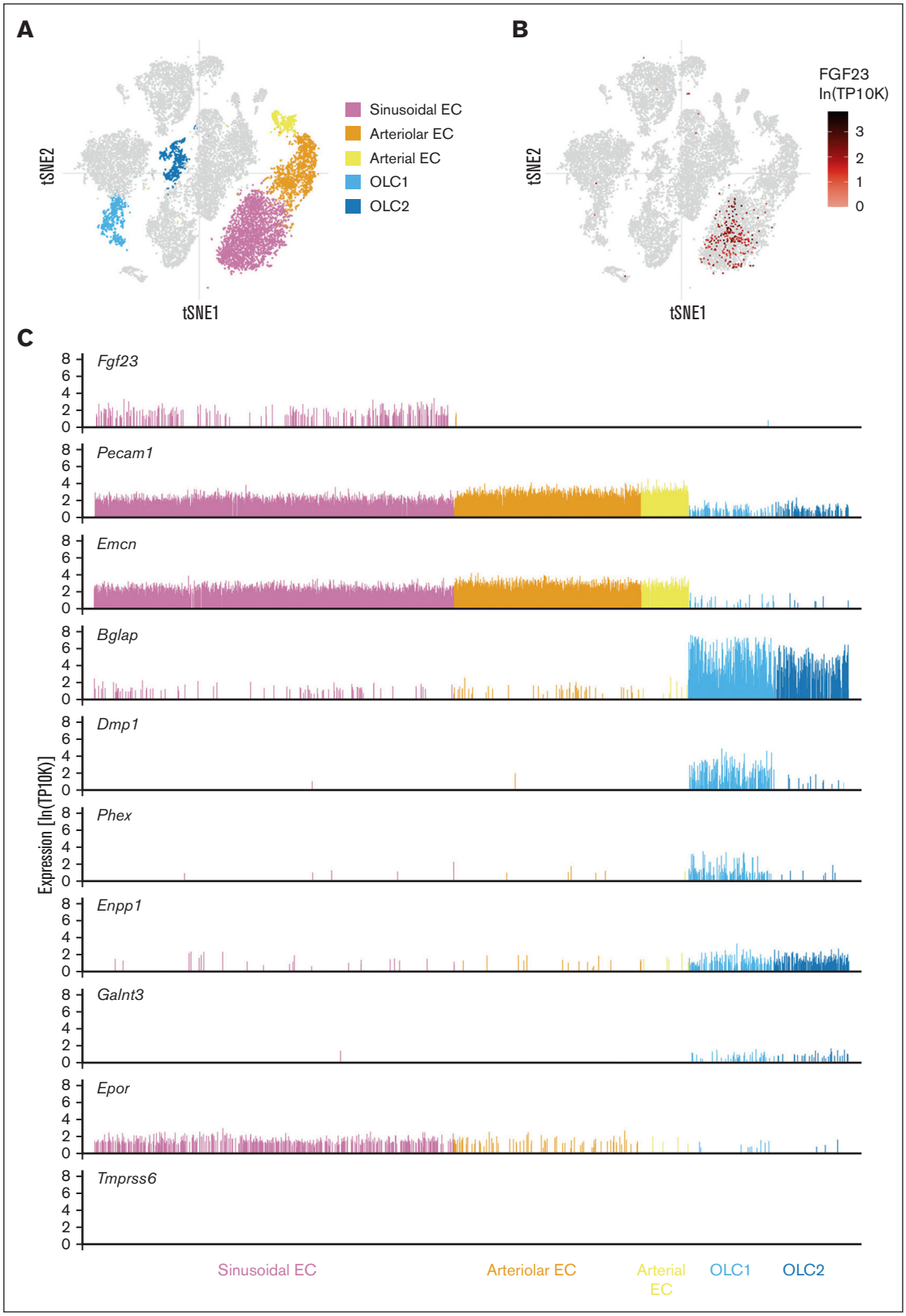

Figure 6. Sinusoidal endothelial cells show higher *Fgf23* expression than other BM stromal cell populations in mice with normal iron balance. Visualization of scRNA-Seq data from 20 896 nonhematopoietic cells (mixed bone and BM fractions) generated by Baryawno et al.[45] Data were downloaded from the Broad Institute Single Cell Portal (https://singlecell.broadinstitute.org/single_cell/study/SCP361/mouse-bone-marrow-stroma-in-homeostasis). T-distributed stochastic neighbor embedding (tSNE) plots (A) highlighting the 5 cell clusters of interest and (B) showing the *Fgf23* expression. (C) The expression of selected genes is shown for each individual cell within the 5 cell clusters highlighted in A. TP10K transcripts per 10 thousand transcripts. EC, endothelial cell; OLC, osteolineage cell.

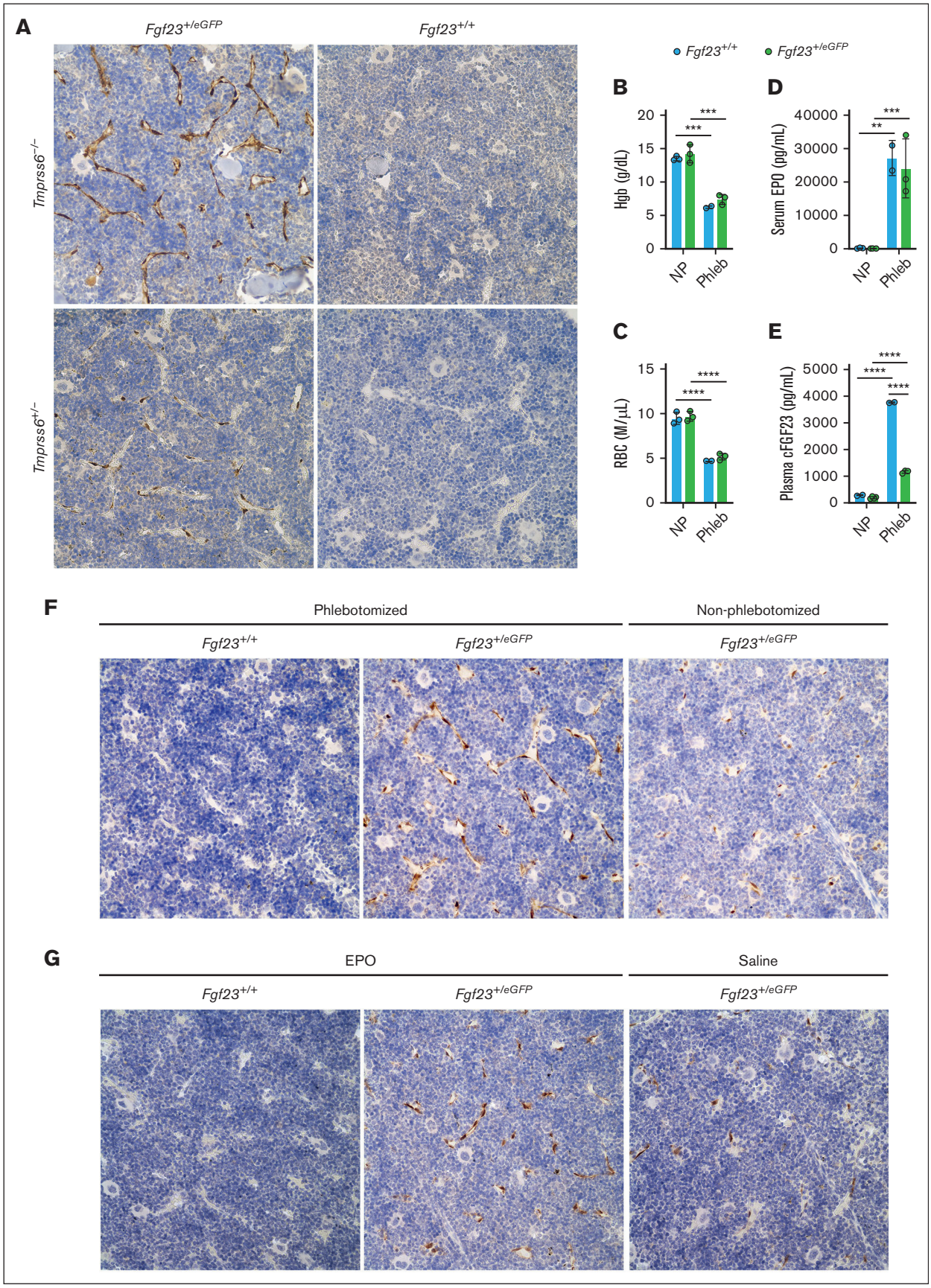
A
Fgf23+/eGFP
Fgf23+/+
Tmprss6−/−
Tmprss6+/−
Fgf23+/+
Fgf23+/eGFP
B
Hgb (g/dL)
20
15
10
5
0
***
***
NP
Phleb
D
Serum EPO (pg/mL)
40000
30000
20000
10000
0
***
**
NP
Phleb
C
RBC (M/μL)
15
10
5
0
****
****
NP
Phleb
E
Plasma cFGF23 (pg/mL)
5000
4000
3000
2000
1000
0
****
****
****
NP
Phleb
F
Phlebotomized
Non-phlebotomized
Fgf23+/+
Fgf23+/eGFP
Fgf23+/eGFP
G
EPO
Saline
Fgf23+/+
Fgf23+/eGFP
Fgf23+/eGFP

Figure 7.

hematopoietic progenitor cells (HPCs) into the circulation.[64] Global *Fgf23*$^{-/-}$ mice and *Fgf23*$^{-/-}$ BM chimeras exhibit impaired HPC mobilization in response to granulocyte colony–stimulating factor (G-CSF) treatment.[64] Additionally, in wild-type mice, G-CSF treatment increased *Fgf23* mRNA levels in the total BM and FGF23 protein levels in the BM extracellular fluid and peripheral blood.[64] After G-CSF treatment, *Fgf23*$^{-/-}$ BM chimeras also showed significant iFGF23 in the BM extracellular fluid, suggesting that nonhematopoietic cells contribute to local iFGF23 levels. In wild-type mice, *Fgf23* mRNA induction was observed in both CD45^{-}Ter-119^{+}CD71^{+} and CD45^{-}Ter-119^{-}cell populations; we note that the latter population is expected to include BM-SECs, raising the possibility that BM-SEC–derived FGF23 may influence HPC mobilization. Indeed, of the different vessel types comprising the BM vascular network, sinusoids are the sites of immature and mature leukocyte trafficking between the BM and circulation.[67] Additionally, the BM microvasculature is a critical component of the hematopoietic stem cell niche.[68,69] In the BM, endothelial cells directly contact stem and progenitor cells, and endothelial cell-derived paracrine factors, known as angiocrine factors, orchestrate the self-renewal and differentiation of stem and progenitor cells.[70] BM-SECs also actively controls erythropoiesis, as illustrated by the impaired terminal erythroid differentiation and fatal anemia observed in mice with selective overexpression of β-catenin in BM-SECs.[71] Interestingly, these mutants also showed elevated serum FGF23 with *Fgf23* mRNA upregulation in BM-SECs, as demonstrated in isolated BM-SECs by quantitative polymerase chain reaction and in BM sections by RNAScope fluorescence in situ hybridization.[71]

In bone, the regulation of FGF23 production involves transcription and translation, posttranslational modification, and cleavage of the mature peptide.[1] Similar to other mouse models with increased erythropoietic drive,[16,43,52,58-61,72] mice in our study with chronic IDA showed markedly increased circulating cFGF23 (intact hormone and C-terminal cleaved fragments) but only modestly increased iFGF23 (intact hormone). Such an ELISA profile has been interpreted to reflect increased FGF23 synthesis offset by increased FGF23 cleavage.[5] This profile may also reflect local consumption of the intact hormone in the BM. Indeed, Ishii et al[64] found that after G-CSF treatment, both iFGF23 and cFGF23 levels were elevated in BM extracellular fluid but only cFGF23 levels were elevated in the circulation.

FGF23 has been found to directly target different cell types in several organs via pathways that may or may not require the coreceptor Klotho.[73] Although *Tmprss6*$^{-/-}$ mice showed elevated urine phosphate-to-creatinine ratios, compatible with the known phosphaturic effects of FGF23, they were not hypophosphatemic (Figure 1M-O). *Tmprss6*$^{-/-}$ bones were brittle, requiring less work to fracture while retaining their stiffness (supplemental Figure 11); this contrasts with the characteristics of bones of *Phex*^{Hyp} mice, which tolerate less force but are pliable.[74] Although FGF23 has been shown to induce left ventricular hypertrophy in mice,[75] *Tmprss6*$^{-/-}$ mice showed cardiomegaly with right ventricular dilatation (supplemental Figure 12), a phenotype observed in mice exposed to chronic hypoxia.[76] Thus, although elevated FGF23 might contribute to abnormal phenotypes in *Tmprss6*$^{-/-}$ mice, we cannot exclude the potential effects of anemia and/or iron deficiency.[77,78]

Several systemic and cellular changes associated with IDA have been proposed and investigated as stimulators of *Fgf23* expression, including decreased iron availability, hypoxia, and elevated EPO levels.[79] In our study, plasma cFGF23 and iFGF23 both showed stronger linear correlations with serum EPO than with serum iron or blood Hgb (Figure 3G-H; supplemental Figure 4C-F). Interestingly, our data mining of scRNA-Seq[45] of BM stroma from wild-type mice detected both *Fgf23* and *Epor* expression in BM-SECs (Figure 6C). Additionally, in nonanemic *Fgf23*$^{+/eGFP}$ mice, we found that direct injection of EPO increased *Fgf23*^{eGFP} reporter expression in BM-SECs relative to vehicle-treated controls (Figure 7G). These findings suggest a model in which elevated circulating levels of EPO, which were observed in both chronic genetically induced IDA and acute phlebotomy-induced anemia, act directly on BM-SECs to promote FGF23 production. Intriguingly, while this manuscript was in revision, Aprile et al[80] reported that EPO treatment upregulates *Fgf23* mRNA via the ERK1/2 and STAT5 pathways in bone-derived cells and TER119-enriched BM cells. Future studies will be required to dissect the mechanisms mediating *Fgf23* upregulation in BM-SECs and the local consequences of FGF23 upregulation in BM-SECs during anemic states. Additionally, it would be interesting to determine whether the induction of circulating FGF23 and hypophosphatemia by certain parenteral iron formulations[81] is mediated by BM-SECs.

Acknowledgments

The authors thank Mark Lessard for confocal imaging, Eileen Chua for technical assistance, and Diane Krause, Vanessa Scanlon, Yi-Chien Lu, Chunliang Xu, and Clemens Bergwitz for helpful discussions. The visual abstract was created with BioRender.com.

Figure 7. BM-SECs are a site of *Fgf23* upregulation in genetically induced IDA, in phlebotomy-induced anemia, and after the direct administration of EPO. (A) Immunohistochemical staining with an anti-GFP antibody in the BM of formalin-fixed, decalcified femur sections of selected *Tmprss6-Fgf23* genotype combinations (6-month-old male mice). Original magnification ×40. Brown staining highlights anti-GFP immunoreactivity; blue staining reflects hematoxylin counterstain. (B-E) Circulating parameters in *Fgf23*$^{+/eGFP}$ and *Fgf23*$^{+/+}$ mice evaluated at the 18-hour time point after a large-volume phlebotomy, compared with nonphlebotomized, genotype-matched controls, validating the expected effects of phlebotomy on (B) Hgb, (C) red blood cell (RBC) count, (D) serum EPO, and (E) plasma cFGF23. *Fgf23*$^{+/eGFP}$ and *Fgf23*$^{+/+}$ female mice (8-weeks-old; 2-4 per group) were either not previously phlebotomized (NP) or underwent a single 500 μL phlebotomy with saline volume replacement 18 hours earlier ("Phleb"). For all graphs, data represent mean ± standard deviation. $^{**}P < .01$; $^{***}P < .001$; and $^{****}P < .0001$ using a two-way ANOVA with Tukey post hoc test. (F) Immunohistochemical staining with anti-GFP antibody in the BM of formalin-fixed, decalcified femur sections harvested 18 hours after a 500 μL phlebotomy (*Fgf23*$^{+/+}$ or *Fgf23*$^{+/eGFP}$ mice) or harvested from nonphlebotomized *Fgf23*$^{+/eGFP}$ control mice. Original magnification ×40. (G) Immunohistochemical staining with anti-GFP antibody in the BM of formalin-fixed decalcified femur sections harvested 6 hours after injection of EPO (*Fgf23*$^{+/+}$ or *Fgf23*$^{+/eGFP}$ mice) or saline vehicle (*Fgf23*$^{+/eGFP}$ control mice). Original magnification ×40.

This work was supported by a Gruber Foundation Gruber Science fellowship (X.L.), American Heart Association Predoctoral fellowship 18PRE33960343 (X.L.), a Burroughs Wellcome Career Award for Medical Scientists (K.E.F.), and National Institutes of Health grant U54 DK106857 (Yale Cooperative Center for Excellence in Hematology).

Authorship

Contribution: X.L., L.L., S.M.T., J.F., and K.E.F. performed the research and analyzed the data; X.L., J.F., and K.E.F. wrote the manuscript and prepared the figures; and K.E.F. supervised the study.

Conflict-of-interest disclosure: The authors declare no competing financial interests.

The current affiliation for X.L. is Department of Cell Biology, Harvard Medical School, Boston, MA.

ORCID profiles: X.L., 0000-0003-1796-8555; S.M.T., 0000-0001-5118-5867; J.F., 0000-0002-6605-869X; K.E.F., 0000-0002-8171-2776.

Correspondence: Karin E. Finberg, Department of Pathology, Yale School of Medicine, 310 Cedar St, PO Box 208023, New Haven, CT 06520-8023; email: karin.finberg@yale.edu.

References

1. Edmonston D, Wolf M. FGF23 at the crossroads of phosphate, iron economy and erythropoiesis. *Nat Rev Nephrol*. 2020;16(1):7-19.
2. Fon Tacer K, Bookout AL, Ding X, et al. Research resource: comprehensive expression atlas of the fibroblast growth factor system in adult mouse. *Mol Endocrinol*. 2010;24(10):2050-2064.
3. Kolek OI, Hines ER, Jones MD, et al. 1alpha,25-dihydroxyvitamin D3 upregulates FGF23 gene expression in bone: the final link in a renal-gastrointestinal-skeletal axis that controls phosphate transport. *Am J Physiol Gastrointest Liver Physiol*. 2005;289(6):G1036-1042.
4. Liu S, Guo R, Simpson LG, Xiao ZS, Burnham CE, Quarles LD. Regulation of fibroblastic growth factor 23 expression but not degradation by PHEX. *J Biol Chem*. 2003;278(39):37419-37426.
5. Wolf M, White KE. Coupling fibroblast growth factor 23 production and cleavage: iron deficiency, rickets, and kidney disease. *Curr Opin Nephrol Hypertens*. 2014;23(4):411-419.
6. Ferrari SL, Bonjour JP, Rizzoli R. Fibroblast growth factor-23 relationship to dietary phosphate and renal phosphate handling in healthy young men. *J Clin Endocrinol Metab*. 2005;90(3):1519-1524.
7. Antoniucci DM, Yamashita T, Portale AA. Dietary phosphorus regulates serum fibroblast growth factor-23 concentrations in healthy men. *J Clin Endocrinol Metab*. 2006;91(8):3144-3149.
8. Ito M, Sakai Y, Furumoto M, et al. Vitamin D and phosphate regulate fibroblast growth factor-23 in K-562 cells. *Am J Physiol Endocrinol Metab*. 2005;288(6):E1101-1109.
9. Shimada T, Hasegawa H, Yamazaki Y, et al. FGF-23 is a potent regulator of vitamin D metabolism and phosphate homeostasis. *J Bone Miner Res*. 2004;19(3):429-435.
10. Burnett-Bowie SAM, Henao MP, Dere ME, Lee H, Leder BZ. Effects of hPTH(1-34) infusion on circulating serum phosphate, 1,25-dihydroxyvitamin D, and FGF23 levels in healthy men. *J Bone Miner Res*. 2009;24(10):1681-1685.
11. Lavi-Moshayoff V, Wasserman G, Meir T, Silver J, Naveh-Many T. PTH increases FGF23 gene expression and mediates the high-FGF23 levels of experimental kidney failure: a bone parathyroid feedback loop. *Am J Physiol Renal Physiol*. 2010;299(4):F882-889.
12. Meir T, Durlacher K, Pan Z, et al. Parathyroid hormone activates the orphan nuclear receptor Nurr1 to induce FGF23 transcription. *Kidney Int*. 2014;86(6):1106-1115.
13. Yamazaki M, Kawai M, Miyagawa K, et al. Interleukin-1-induced acute bone resorption facilitates the secretion of fibroblast growth factor 23 into the circulation. *J Bone Miner Metab*. 2015;33(3):342-354.
14. Ito N, Wijenayaka AR, Prideaux M, et al. Regulation of FGF23 expression in IDG-SW3 osteocytes and human bone by pro-inflammatory stimuli. *Mol Cell Endocrinol*. 2015;399:208-218.
15. Onal M, Carlson AH, Thostenson JD, et al. A novel distal enhancer mediates inflammation-PTH-and early onset murine kidney disease-induced expression of the mouse Fgf23 gene. *JBMR Plus*. 2018;2(1):32-47.
16. David V, Martin A, Isakova T, et al. Inflammation and functional iron deficiency regulate fibroblast growth factor 23 production. *Kidney Int*. 2016;89(1):135-146.
17. McKnight Q, Jenkins S, Li X, et al. IL-1beta drives production of FGF-23 at the onset of chronic kidney disease in mice. *J Bone Miner Res*. 2020;35(7):1352-1362.
18. Durlacher-Betzer K, Hassan A, Levi R, Axelrod J, Silver J, Naveh-Many T. Interleukin-6 contributes to the increase in fibroblast growth factor 23 expression in acute and chronic kidney disease. *Kidney Int*. 2018;94(2):315-325.
19. Musgrove J, Wolf M. Regulation and effects of FGF23 in chronic kidney disease. *Annu Rev Physiol*. 2020;82(1):365-390.
20. White KE, Evans WE, O'Riordan JL, et al. Autosomal dominant hypophosphataemic rickets is associated with mutations in FGF23. *Nat Genet*. 2000;26(3):345-348.
21. Imel EA, Hui SL, Econs MJ. FGF23 concentrations vary with disease status in autosomal dominant hypophosphatemic rickets. *J Bone Miner Res*. 2007;22(4):520-526.

22. Imel EA, Peacock M, Gray AK, Padgett LR, Hui SL, Econs MJ. Iron modifies plasma FGF23 differently in autosomal dominant hypophosphatemic rickets and healthy humans. *J Clin Endocrinol Metab*. 2011;96(11):3541-3549.

23. Imel EA, Liu Z, McQueen AK, et al. Serum fibroblast growth factor 23, serum iron and bone mineral density in premenopausal women. *Bone*. 2016;86: 98-105.

24. Fernandez-Real JM, Puig J, Serrano M, et al. Iron and obesity status-associated insulin resistance influence circulating fibroblast-growth factor-23 concentrations. *PLoS One*. 2013;8(3):e58961.

25. Lewerin C, Ljunggren O, Nilsson-Ehle H, et al. Low serum iron is associated with high serum intact FGF23 in elderly men: the Swedish MrOS study. *Bone*. 2017;98:1-8.

26. Bożentowicz-Wikarek M, Kocełak P, Owczarek A, et al. Plasma fibroblast growth factor 23 concentration and iron status. Does the relationship exist in the elderly population? *Clin Biochem*. 2015;48(6):431-436.

27. Braithwaite VS, Mwangi MN, Jones KS, et al. Antenatal iron supplementation, FGF23, and bone metabolism in Kenyan women and their offspring: secondary analysis of a randomized controlled trial. *Am J Clin Nutr*. 2021;113(5):1104-1114.

28. Farrow EG, Yu X, Summers LJ, et al. Iron deficiency drives an autosomal dominant hypophosphatemic rickets (ADHR) phenotype in fibroblast growth factor-23 (Fgf23) knock-in mice. *Proc Natl Acad Sci U S A*. 2011;108(46):E1146-1155.

29. Clinkenbeard EL, Farrow EG, Summers LJ, et al. Neonatal iron deficiency causes abnormal phosphate metabolism by elevating FGF23 in normal and ADHR mice. *J Bone Miner Res*. 2014;29(2):361-369.

30. Finberg KE, Heeney MM, Campagna DR, et al. Mutations in TMPRSS6 cause iron-refractory iron deficiency anemia (IRIDA). *Nat Genet*. 2008;40(5): 569-571.

31. Ramsay AJ, Reid JC, Velasco G, Quigley JP, Hooper JD. The type II transmembrane serine protease matriptase-2–identification, structural features, enzymology, expression pattern and potential roles. *Front Biosci*. 2008;13(2):569-579.

32. Du X, She E, Gelbart T, et al. The serine protease TMPRSS6 is required to sense iron deficiency. *Science*. 2008;320(5879):1088-1092.

33. Finberg KE, Whittlesey RL, Fleming MD, Andrews NC. Down-regulation of Bmp/Smad signaling by Tmprss6 is required for maintenance of systemic iron homeostasis. *Blood*. 2010;115(18):3817-3826.

34. Willemetz A, Lenoir A, Deschemin JC, et al. Matriptase-2 is essential for hepcidin repression during fetal life and postnatal development in mice to maintain iron homeostasis. *Blood*. 2014;124(3):441-444.

35. Riba M, Rausa M, Sorosina M, et al. A strong anti-inflammatory signature revealed by liver transcription profiling of Tmprss6−/− mice. *PLoS One*. 2013; 8(7):e69694.

36. Xavier-Ferrucio J, Scanlon V, Li X, et al. Low iron promotes megakaryocytic commitment of megakaryocytic-erythroid progenitors in humans and mice. *Blood*. 2019;134(18):1547-1557.

37. Liu S, Zhou J, Tang W, Jiang X, Rowe DW, Quarles LD. Pathogenic role of Fgf23 in Hyp mice. *Am J Physiol Endocrinol Metab*. 2006;291(1):E38-49.

38. Li X, Lozovatsky L, Sukumaran A, et al. NCOA4 is regulated by HIF and mediates mobilization of murine hepatic iron stores after blood loss. *Blood*. 2020;136(23):2691-2702.

39. Torrance JD, Bothwell TH. Tissue iron stores. In: Cook JD, ed. *Methods in Hematology: Iron*. Vol. 1. New York: Churchill Livingstone; 1980:90-115.

40. Stagg DB, Whittlesey RL, Li X, et al. Genetic loss of Tmprss6 alters terminal erythroid differentiation in a mouse model of beta-thalassemia intermedia. *Haematologica*. 2019;104(10):e442-e446.

41. Xu C, Gao X, Wei Q, et al. Stem cell factor is selectively secreted by arterial endothelial cells in bone marrow. *Nat Commun*. 2018;9(1):2449.

42. Finberg KE, Whittlesey RL, Andrews NC. Tmprss6 is a genetic modifier of the Hfe-hemochromatosis phenotype in mice. *Blood*. 2011;117(17): 4590-4599.

43. Rabadi S, Udo I, Leaf DE, Waikar SS, Christov M. Acute blood loss stimulates fibroblast growth factor 23 production. *Am J Physiol Renal Physiol*. 2018; 314(1):F132-F139.

44. Zhang G, Yang X, Gao R. Research progress on the structure and function of endomucin. *Animal Model Exp Med*. 2020;3(4):325-329.

45. Baryawno N, Przybylski D, Kowalczyk MS, et al. A cellular taxonomy of the bone marrow stroma in homeostasis and leukemia. *Cell*. 2019;177(7): 1915-1932.e16.

46. Feng JQ, Ward LM, Liu S, et al. Loss of DMP1 causes rickets and osteomalacia and identifies a role for osteocytes in mineral metabolism. *Nat Genet*. 2006;38(11):1310-1315.

47. Lorenz-Depiereux B, Schnabel D, Tiosano D, Hausler G, Strom TM. Loss-of-function ENPP1 mutations cause both generalized arterial calcification of infancy and autosomal-recessive hypophosphatemic rickets. *Am J Hum Genet*. 2010;86(2):267-272.

48. Ichikawa S, Baujat G, Seyahi A, et al. Clinical variability of familial tumoral calcinosis caused by novel GALNT3 mutations. *Am J Med Genet A*. 2010; 152A(4):896-903.

49. Helbling PM, Pineiro-Yanez E, Gerosa R, et al. Global transcriptomic profiling of the bone marrow stromal microenvironment during postnatal development, aging, and inflammation. *Cell Rep*. 2019;29(10):3313-3330.e4.

50. Brazelton TR, Blau HM. Optimizing techniques for tracking transplanted stem cells in vivo. *Stem Cells*. 2005;23(9):1251-1265.

51. Kautz L, Jung G, Valore EV, Rivella S, Nemeth E, Ganz T. Identification of erythroferrone as an erythroid regulator of iron metabolism. *Nat Genet*. 2014; 46(7):678-684.

52. Hanudel MR, Eisenga MF, Rappaport M, et al. Effects of erythropoietin on fibroblast growth factor 23 in mice and humans. *Nephrol Dial Transplant*. 2019;34(12):2057-2065.

53. Clinkenbeard EL, Cass TA, Ni P, et al. Conditional deletion of murine Fgf23: interruption of the normal skeletal responses to phosphate challenge and rescue of genetic hypophosphatemia. *J Bone Miner Res*. 2016;31(6):1247-1257.

54. Clinkenbeard EL, Noonan ML, Thomas JC, et al. Increased FGF23 protects against detrimental cardio-renal consequences during elevated blood phosphate in CKD. *JCI Insight*. 2019;4(4):e123817.

55. Yuan B, Takaiwa M, Clemens TL, et al. Aberrant Phex function in osteoblasts and osteocytes alone underlies murine X-linked hypophosphatemia. *J Clin Invest*. 2008;118(2):722-734.

56. Eicher EM, Southard JL, Scriver CR, Glorieux FH. Hypophosphatemia: mouse model for human familial hypophosphatemic (vitamin D-resistant) rickets. *Proc Natl Acad Sci U S A*. 1976;73(12):4667-4671.

57. Beck L, Soumounou Y, Martel J, et al. Pex/PEX tissue distribution and evidence for a deletion in the 3' region of the Pex gene in X-linked hypophosphatemic mice. *J Clin Invest*. 1997;99(6):1200-1209.

58. Flamme I, Ellinghaus P, Urrego D, Kruger T. FGF23 expression in rodents is directly induced via erythropoietin after inhibition of hypoxia inducible factor proline hydroxylase. *PLoS One*. 2017;12(10):e0186979.

59. Clinkenbeard EL, Hanudel MR, Stayrook KR, et al. Erythropoietin stimulates murine and human fibroblast growth factor-23, revealing novel roles for bone and bone marrow. *Haematologica*. 2017;102(11):e427-e430.

60. Daryadel A, Bettoni C, Haider T, et al. Erythropoietin stimulates fibroblast growth factor 23 (FGF23) in mice and men. *Pflugers Arch*. 2018;470(10):1569-1582.

61. Toro L, Barrientos V, Leon P, et al. Erythropoietin induces bone marrow and plasma fibroblast growth factor 23 during acute kidney injury. *Kidney Int*. 2018;93(5):1131-1141.

62. Shimada T, Kakitani M, Yamazaki Y, et al. Targeted ablation of Fgf23 demonstrates an essential physiological role of FGF23 in phosphate and vitamin D metabolism. *J Clin Invest*. 2004;113(4):561-568.

63. Coe LM, Madathil SV, Casu C, Lanske B, Rivella S, Sitara D. FGF-23 is a negative regulator of prenatal and postnatal erythropoiesis. *J Biol Chem*. 2014;289(14):9795-9810.

64. Ishii S, Suzuki T, Wakahashi K, et al. FGF-23 from erythroblasts promotes hematopoietic progenitor mobilization. *Blood*. 2021;137(11):1457-1467.

65. Slayton WB, Li XM, Butler J, et al. The role of the donor in the repair of the marrow vascular niche following hematopoietic stem cell transplant. *Stem Cells*. 2007;25(11):2945-2955.

66. Li XM, Hu Z, Jorgenson ML, Wingard JR, Slayton WB. Bone marrow sinusoidal endothelial cells undergo nonapoptotic cell death and are replaced by proliferating sinusoidal cells in situ to maintain the vascular niche following lethal irradiation. *Exp Hematol*. 2008;36(9):1143-1156.

67. Itkin T, Gur-Cohen S, Spencer JA, et al. Distinct bone marrow blood vessels differentially regulate haematopoiesis. *Nature*. 2016;532(7599):323-328.

68. Pinho S, Frenette PS. Haematopoietic stem cell activity and interactions with the niche. *Nat Rev Mol Cell Biol*. 2019;20(5):303-320.

69. Comazzetto S, Shen B, Morrison SJ. Niches that regulate stem cells and hematopoiesis in adult bone marrow. *Dev Cell*. 2021;56(13):1848-1860.

70. Rafii S, Butler JM, Ding BS. Angiocrine functions of organ-specific endothelial cells. *Nature*. 2016;529(7586):316-325.

71. Heil J, Olsavszky V, Busch K, et al. Bone marrow sinusoidal endothelium controls terminal erythroid differentiation and reticulocyte maturation. *Nat Commun*. 2021;12(1):6963.

72. Hanudel MR, Chua K, Rappaport M, et al. Effects of dietary iron intake and chronic kidney disease on fibroblast growth factor 23 metabolism in wild-type and hepcidin knockout mice. *Am J Physiol Renal Physiol*. 2016;311(6):F1369-F1377.

73. Richter B, Faul C. FGF23 actions on target tissues-with and without klotho. *Front Endocrinol (Lausanne)*. 2018;9:189.

74. Liu S, Brown TA, Zhou J, et al. Role of matrix extracellular phosphoglycoprotein in the pathogenesis of X-linked hypophosphatemia. *J Am Soc Nephrol*. 2005;16(6):1645-1653.

75. Faul C, Amaral AP, Oskouei B, et al. FGF23 induces left ventricular hypertrophy. *J Clin Invest*. 2011;121(11):4393-4408.

76. Yet SF, Perrella MA, Layne MD, et al. Hypoxia induces severe right ventricular dilatation and infarction in heme oxygenase-1 null mice. *J Clin Invest*. 1999;103(8):R23-29.

77. Balogh E, Paragh G, Jeney V. Influence of iron on bone homeostasis. *Pharmaceuticals (Basel)*. 2018;11(4):107.

78. Zhang H, Zhabyeyev P, Wang S, Oudit GY. Role of iron metabolism in heart failure: From iron deficiency to iron overload. *Biochim Biophys Acta Mol Basis Dis*. 2019;1865(7):1925-1937.

79. Ratsma DMA, Zillikens MC, van der Eerden BCJ. Upstream regulators of fibroblast growth factor 23. *Front Endocrinol (Lausanne)*. 2021;12:588096.

80. Aprile A, Raggi L, Bolamperti S, et al. Inhibition of FGF23 is a therapeutic strategy to target hematopoietic stem cell niche defects in beta-thalassemia. *Sci Transl Med*. 2023;15(698):eabq3679.

81. Schaefer B, Tobiasch M, Wagner S, et al. Hypophosphatemia after intravenous iron therapy: Comprehensive review of clinical findings and recommendations for management. *Bone*. 2022;154:116202.

82. Meyer RA Jr, Meyer MH, Gray RW. Parabiosis suggests a humoral factor is involved in X-linked hypophosphatemia in mice. *J Bone Miner Res*. 1989;4(4):493-500.